Suppression of the Shh pathway using a small molecule inhibitor eliminates medulloblastoma in *Ptc1*$^{+/-}$*p53*$^{-/-}$ mice

Justyna T. Romer,[1] Hiromichi Kimura,[1] Susan Magdaleno,[1] Ken Sasai,[1] Christine Fuller,[1] Helen Baines,[1] Michele Connelly,[1] Clinton F. Stewart,[1] Stephen Gould,[2] Lee L. Rubin,[2] and Tom Curran[1,*]

[1]Department of Developmental Neurobiology, St. Jude Children's Research Hospital, Memphis, Tennessee 38105
[2]Curis, Inc., Cambridge, Massachusetts 02478
*Correspondence: tom.curran@stjude.org

Summary

Medulloblastoma is the most common malignant pediatric brain tumor. Current treatment is associated with major long-term side effects; therefore, new nontoxic therapies, targeting specific molecular defects in this cancer, need to be developed. We use a mouse model of medulloblastoma to show that inhibition of the Sonic Hedgehog (Shh) pathway provides a novel therapy for medulloblastoma. A small molecule inhibitor of the Shh pathway, HhAntag, blocked the function of Smoothened in mice with medulloblastoma. This resulted in suppression of several genes highly expressed in medulloblastoma, inhibition of cell proliferation, increase in cell death and, at the highest dose, complete eradication of tumors. Long-term treatment with HhAntag prolonged medulloblastoma-free survival. These findings support the development of Shh antagonists for the treatment of medulloblastoma.

Introduction

Research in molecular oncology has benefited from the advent of mouse models of human cancer (Hesselager and Holland, 2003; Van Dyke and Jacks, 2002). Genetically engineered mouse strains have been used to investigate tumor etiology and to elaborate the molecular pathways that contribute to human cancer. However, the greatest potential application of such models is to pioneer the development of novel therapies that are specifically targeted against growth control pathways altered in cancer. For this purpose, it is necessary that mouse models recapitulate both the genetics and the biology of the corresponding human disease. It is also critical that the tumor incidence is high and the age of onset is predictable, to ensure that cohorts of mice bearing tumors can be identified and treated with potential anticancer drugs. Previously, we developed a high incidence mouse model for the pediatric brain tumor medulloblastoma (Wetmore et al., 2001). Medulloblastoma, a primitive neuroectodermal tumor, arises in the cerebellum and accounts for approximately 20% of all pediatric brain tumors. Current treatment involves surgical resection, chemotherapy, and radiation of the craniospinal axis (Ellison et al., 2003). Although the overall 5 year survival rate is approximately 70%, treatment is associated with long-term side effects including ataxia, neuroendocrine problems, intellectual deterioration, and neuropsychological difficulties (Chintagumpala et al., 2001; Ellison et al., 2003). There is a critical need for new, nontoxic therapies for medulloblastoma.

The first indication that alteration in the Shh pathway contributes to medulloblastoma formation was the discovery that germline mutations in the Shh receptor, *Patched-1* (*PTCH1*), underlie the human developmental disorder Gorlin syndrome (Gorlin, 1995; Hahn et al., 1996; Johnson et al., 1996). Gorlin syndrome, also known as Basal Cell Nevus Syndrome, is characterized by large body size, developmental and skeletal abnormalities, fibromas of soft tissue, radiation sensitivity, basal cell carcinoma, and increased incidence of medulloblastoma (Goodrich and Scott, 1998; Kimonis et al., 1997). Heterozygous loss of *PTCH1* occurs in approximately 10% of sporadic human medulloblastoma (Ellison et al., 2003; Wechsler-Reya and Scott, 2001), and mutations in downstream components of the Shh pathway, Smoothened (*SMOH*) and Suppressor of Fused (*SUFU*), which lead to activation of the pathway, have also been described (Reifenberger et al., 1998; Taylor et al., 2002). In mice, heterozygous mutation of *Patched-1* (*Ptc1*) is associated with an approximately 20% incidence of medulloblastoma over a period of 1 year (Corcoran and Scott, 2001; Goodrich et al., 1997; Wetmore et al., 2000). We accelerated the incidence and decreased the latency of medulloblastoma by crossing *Ptc1*$^{+/-}$ mice with *p53*$^{-/-}$ mice (Wetmore et al., 2001). *Ptc1*$^{+/-}$*p53*$^{-/-}$ mice develop medulloblastoma and most die from brain tumors within 12 weeks of birth. *P53* is mutated in approximately 10% of human

SIGNIFICANCE

Therapy for pediatric cancers of the CNS has not improved significantly in the last three decades. This is partly due to the absence of adequate model systems for testing novel therapies. Current models are based on xenografts, allografts, or in vitro culture of human tumor cells. In these models, the cancer cells are removed from their normal environment, undergo selective pressure, and may not be representative of the original tumor. Cancer models should recapitulate the causative genetic lesions and the anatomical location and developmental time frame of the corresponding human disease. Here, we use such a model to test a novel therapy for medulloblastoma; we show that suppression of the Sonic Hedgehog pathway can be an effective treatment for this tumor.

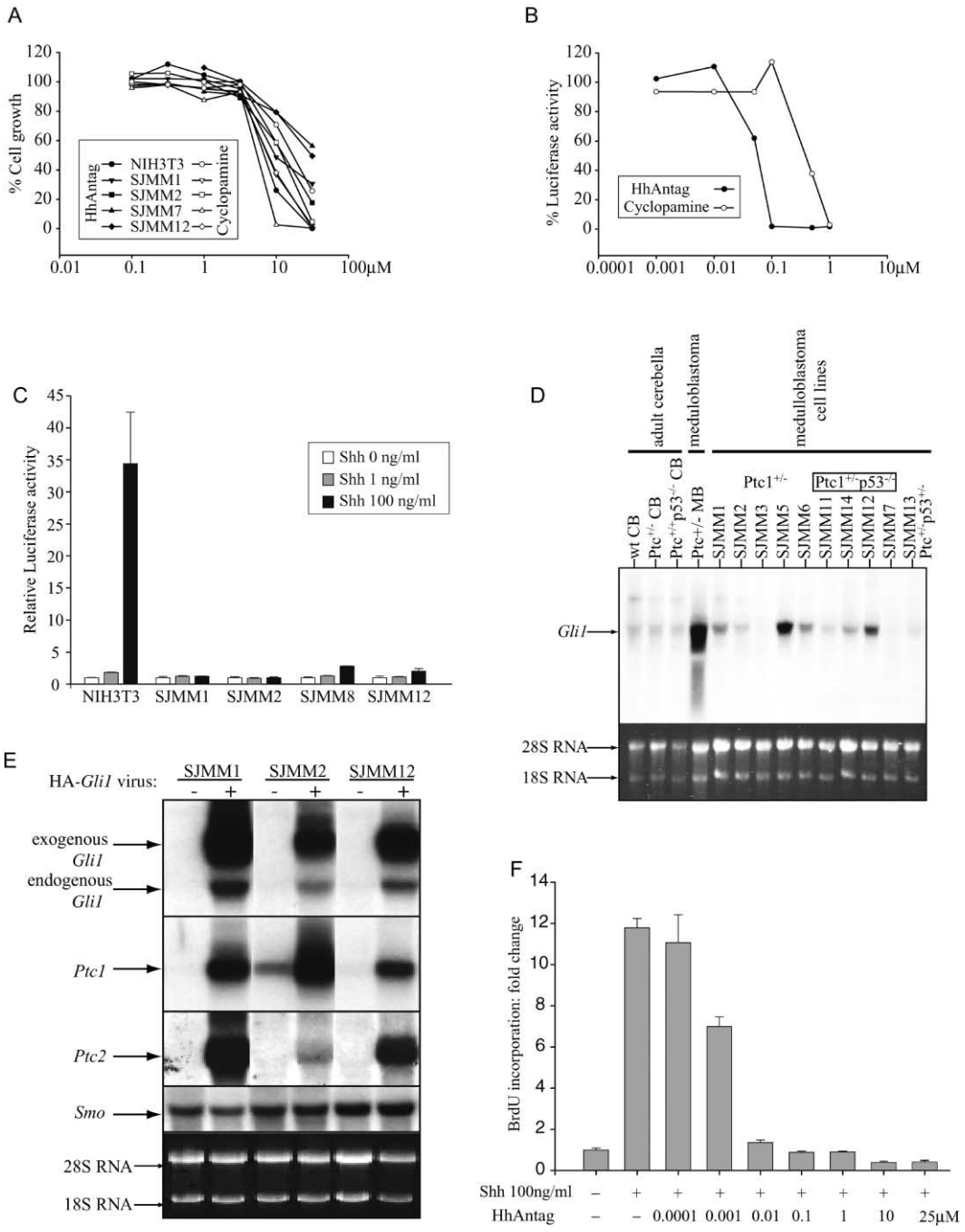

Figure 1. The Shh pathway is downregulated in cultured medulloblastoma cells

A: HhAntag and cyclopamine inhibit growth of cultured NIH3T3 and medulloblastoma cells at similar concentrations. The graph shows the percentile change in cell growth, as determined by Alamar blue staining, following treatment of cells with increasing concentrations of HhAntag or cyclopamine. The medulloblastoma cell cultures, SJMM1 and SJMM2, were derived from *Ptc1*$^{+/-}$ tumors, whereas SJMM7 and SJMM12 were derived from *Ptc1*$^{+/-}$*p53*$^{-/-}$ tumors.

B: The Shh pathway was activated in NIH3T3 cells containing a *Gli*-luciferase reporter by treatment with 100 ng/ml ShhN, and the inhibitory effects of HhAntag and cyclopamine were compared. HhAntag is >10 times better than cyclopamine at inhibiting Shh activity. Note that the concentration of HhAntag required to inhibit cell growth is approximately 1000-fold higher than that needed to suppress Shh activity.

C: Shh induces *Gli*-luciferase activity in NIH3T3 cells but not in medulloblastoma cell cultures. Medulloblastoma cultures and NIH3T3 cells transfected with a *Gli*-luciferase reporter plasmid were treated with increasing doses of Shh.

D: *Gli1* is highly expressed in medulloblastoma in vivo but is downregulated in cell lines derived from tumors. Total RNA, isolated from normal cerebella, medulloblastoma, or medulloblastoma cultures, was analyzed by hybridization to a *Gli1* probe. Ethidium bromide staining of the 28S and 18S rRNA is shown as a loading control.

E: Gli1 can activate target genes in medulloblastoma cells. Cells were infected with a retroviral vector expressing an HA-tagged full-length *Gli1* cDNA. RNA was isolated and analyzed by hybridization to probes specific for *Gli1*, *Ptc1*, *Ptc2*, and *Smo*. Ethidium bromide staining of the 28S and 18S rRNA is shown as a loading control.

medulloblastoma, and the P53 pathway is defective in a larger subset of tumors (Ellison, 2002; Frank et al., 2004; Kleihues et al., 1997). In addition, germline mutations of *P53* are associated with medulloblastoma in Li-Fraumeni syndrome (Malkin et al., 1990). Thus, $Ptc1^{+/-}p53^{-/-}$ mice provide a useful model to develop novel therapies for brain tumors, targeted against the Shh pathway.

During brain development, Shh released by migrating Purkinje cells binds to Ptc1 present on granule neuron precursor (GNP) cells in the external germinal layer (EGL) of the cerebellum (Wechsler-Reya and Scott, 2001). This interaction causes derepression of Smoothened (Smo) (Taipale et al., 2002) and increased expression of transcription factor *Gli1* and proliferation of GNP cells. The Shh pathway is critical during embryogenesis but is downregulated after early postnatal development in most tissues, including the brain. In contrast, more than 30% of human medulloblastoma exhibit high levels of *GLI1* expression (Lee et al., 2003), indicating that abnormal activation of the Shh pathway is important in a subset of pediatric brain tumors. Thus, the Shh pathway is a potential therapeutic target for development of novel treatments for medulloblastoma.

Cyclopamine, an alkaloid isolated from the corn lily *Veratrum californicum* (Binns et al., 1963; Keeler and Binns, 1968), has been shown to suppress the response of target tissues to Shh (Cooper et al., 1998) by binding to Smo (Chen et al., 2002). Recent observations suggest that cyclopamine inhibits the growth of cultured medulloblastoma cells and allografts by inhibiting Smo (Berman et al., 2002). However, cyclopamine is not a good drug candidate for treatment of medulloblastoma because it has a relatively low affinity for Smo. High-throughput, cell-based screening assays identified several small molecule inhibitors of the Shh pathway (Williams et al., 2003). One of these compounds, a benzimidazole derivative, Hh-Antag691, here referred to as HhAntag (Gabay et al., 2003), exhibited higher affinity for Smo than cyclopamine, blocking Shh function at >10-fold lower concentrations. HhAntag penetrates the blood-brain barrier after oral delivery, making it an ideal candidate for treatment of brain tumors caused by increased activity of Smo. Therefore, we selected HhAntag to treat medulloblastoma in $Ptc1^{+/-}p53^{-/-}$ mice. We found that HhAntag inhibited *Gli1* expression in a dose-dependent manner in tumor tissue in vivo. Treatment of tumor-bearing mice twice daily with HhAntag at 20 or 100 mg/kg of body weight, by oral gavage, for 4 days, inhibited tumor cell proliferation and increased apoptosis. Twice daily treatment of mice for 2 weeks with 20 mg/kg of HhAntag resulted in reduction of tumor volume, and complete elimination of tumors was observed in mice treated with 100 mg/kg HhAntag. In longer-term studies, 100 mg/kg HhAntag given once a day significantly enhanced brain tumor-free survival. These results suggest that HhAntag may be beneficial for treatment of medulloblastoma and other tumors in which the Shh pathway is deregulated.

Results

HhAntag blocks Shh signaling at concentrations that do not affect cell growth

As a first step in analyzing the ability of HhAntag to block medulloblastoma growth, we treated cultured tumor cells derived from $Ptc1^{+/-}$ and $Ptc1^{+/-}p53^{-/-}$ mice as well as NIH3T3 cells with increasing concentrations of HhAntag or cyclopamine. We measured the effects on cell growth, as determined by Alamar blue staining, and found that both compounds exhibited similar IC_{50} values in growth assays (10–30 μM), with growth of some medulloblastoma cultures inhibited more readily by cyclopamine than HhAntag (Figure 1A). Similar results were obtained when we used cell counts as a measure of proliferation. Next, we looked at the concentration of HhAntag and cyclopamine required to suppress the Shh pathway. We transfected NIH3T3 cells with a *Gli*-luciferase reporter construct and measured inhibition of the Shh pathway by the two compounds following maximal stimulation by Shh (Figure 1B). HhAntag was significantly more potent than cyclopamine at suppressing Shh signaling; it exhibited an EC_{50} of 0.04 μM compared to 0.5 μM for cyclopamine (Figure 1B). Surprisingly, the drug concentrations required to block cell growth were higher than those required to inhibit Smo activity by approximately 100- and 1000-fold for cyclopamine and HhAntag, respectively. Indeed, both HhAntag and cyclopamine were able to completely suppress Shh activation of *Gli*-luciferase in NIH3T3 cells at concentrations that did not affect cell growth. These results support the selection of HhAntag as a potent Smo inhibitor for preclinical studies on medulloblastoma. However, they also raise the concern that growth inhibition in cell culture may not be related to inhibition of Smo, as the concentrations that suppressed the Shh pathway were 100- to 1000-fold lower than those that inhibited cell growth.

The Shh pathway is not active in cultured medulloblastoma cells

To investigate the status of the Shh pathway in cultured medulloblastoma cells, we treated NIH3T3 cells and medulloblastoma cultures containing a *Gli*-luciferase construct with Shh (Figure 1C). Although NIH3T3 cells exhibited a strong dose-dependent increase in luciferase activity in response to Shh, all of the medulloblastoma cultures failed to respond. Previously, we reported that medulloblastomas express high levels of *Gli1,* indicating that the Shh pathway is active in tumors in vivo (Wetmore et al., 2001). However, examination of mRNA levels in cultured medulloblastoma cells revealed that *Gli1* mRNA was much reduced or absent in vitro (Figure 1D). To ensure that the downstream components of the Shh pathway were intact in medulloblastoma cell cultures, we confirmed the presence of normal *Smo* and *Ptc1* mRNA by sequencing cDNA derived from tumor cell RNA. In addition, we demonstrated that ectopic expression of *Gli1,* using a retroviral vector, increased expression of the endogenous target genes *Gli1*, *Ptc1*, and *Ptc2* (Figure 1E). These findings demonstrate that the Shh pathway is suppressed in

F: HhAntag efficiently blocks Shh-induced proliferation of GNP cells in a dose-dependent manner. GNP cells, isolated from postnatal day 6 mice, were treated with 100 ng/ml ShhN in the presence of increasing concentrations of HhAntag. Cell proliferation was measured by determining the fold difference in BrdU incorporation, relative to incorporation in the absence of Shh. Note, much lower concentrations of HhAntag block growth of GNP cells than those required to block growth of medulloblastoma cells in culture.

cultured medulloblastoma cells at a step between Smo and Gli1 and they imply that growth inhibition caused by exposure to cyclopamine and HhAntag in vitro (Figure 1A) is not mediated by inactivation of Smo. In contrast to the high concentration of drug required to inhibit growth of medulloblastoma and NIH3T3 cells, HhAntag efficiently blocked Shh-mediated proliferation of GNP cells at the same low concentrations that inhibited *Gli*-luciferase activity (Figure 1F). Thus, it is possible that additional factors present in the intracranial environment and absent in culture are needed to maintain the ability of medulloblastoma cells to respond to Shh.

HhAntag inhibits the Shh pathway in medulloblastoma cells in vivo

The results presented above indicate that Smo activity is not required for proliferation of medulloblastoma cells in culture. To determine if Smo activity can be blocked in tumor cells in vivo, we analyzed *Gli1* expression in *Ptc1*$^{+/-}$*p53*$^{-/-}$ mice treated with HhAntag. Cohorts of mutant mice were treated with HhAntag, administered twice daily by oral gavage, for 4 days, at 20 or 100 mg/kg of body weight. To control for nonspecific effects, we also treated a cohort of mutant mice with vehicle. Treatment was initiated in 6-week-old *Ptc1*$^{+/-}$*p53*$^{-/-}$ mice, as they contain substantial tumor mass at this age. At the end of the dosing regimen, mice were euthanized and total RNA was isolated from tumor tissue together with the entire cerebellum. This approach reduces sampling errors that would be introduced by attempting to dissect tumor tissue free from normal cerebellum. Tumors in *Ptc*$^{+/-}$*p53*$^{-/-}$ mice arise in very young mice, and they are intimately associated with normal cerebellar structure. By combining tumor tissue and the complete cerebellum, we ensure that the normal component of each sample is constant and the differences observed in gene expression reflect changes in tumor cells. We also measured the level of HhAntag in the remaining brain tissue to confirm that the compound penetrated the blood-brain barrier. The mice treated with 20 and 100 mg/kg of HhAntag contained an average of 0.38 and 2.0 mg/kg of drug, respectively, and no compound was detected in vehicle-treated mice (Figure 2A).

Quantitative real-time PCR analysis of *Gli1* expression levels revealed extensive variation among control samples (Figure 2A). This was expected, as the time of tumor development and tumor growth rate vary among individual mice in this spontaneous brain tumor model. Therefore, we used the Exact Kruskal-Wallis test to determine whether the results reflected significant differences in gene expression among the different treatment groups (Figure 2B). HhAntag effectively suppressed *Gli1* mRNA levels in a dose-dependent manner in vivo (Figures 2A and 2B). In addition to *Gli1*, we examined the levels of several other genes (*Sfrp1*, *Math1*, and *Ptc2*) previously identified to be highly expressed in *Ptc1*$^{+/-}$*p53*$^{-/-}$ medulloblastoma (Lee et al., 2003). We found a dose-dependent decrease in mRNA levels of these genes in response to HhAntag (Figure 2B). As a control, we examined expression of *Reln*, which is present in GNP and tumor cells (Wetmore et al., 2000) but is not known to be under control of the Shh pathway. The *Reln* levels were not affected by drug treatment (Figure 2B). Surprisingly, transcription of the wild-type allele of *Ptc1,* which like *Gli1* is a target of Shh signaling, was unaffected by drug treatment (Figure 2B). Previously, we demonstrated that both the normal and the mutated *Ptc1* alleles are expressed in *Ptc1*$^{+/-}$ medulloblastoma cells at levels comparable to that in normal developing cerebellum (Wetmore et al., 2000). This agrees with the original report from Goodrich et al. (1997) demonstrating expression of the mutated *Ptc1* allele in tumor cell by β-gal staining. Thus, although *Ptc1* expression has been used to monitor the response of mouse medulloblastoma cells to Smo inhibition in vitro (Berman et al., 2002), it appears that *Ptc1* is not a target of the Shh pathway in these tumor cells in vivo.

The reduction in mRNA levels of Shh pathway target genes observed in the short-term study was not simply due to loss of tumor mass following treatment with HhAntag, as histological analyses of cerebella from treated mice indicated that tumors were present in all treated mice. To confirm that gene expression was decreased in tumor cells in vivo, we conducted in situ hybridization analyses of brain sections using probes specific for *Gli1, Sfrp1, Math1, Ptc1, Ptc2*, and *Reln* genes (Figure 3). Consistent with the quantitative PCR analysis, we found that *Gli1, Sfrp1, Math1*, and *Ptc2* were expressed mostly in the tumor cells and not in the adjacent normal cerebellum. There was a marked decrease in expression of all of these genes in response to 20 mg/kg of HhAntag and a complete absence of expression following treatment with 100 mg/kg, despite the presence of substantial tumor mass (Figure 3). When the decrease in gene expression levels between vehicle and 100 mg/kg HhAntag-treated mice (7- to 300-fold changes, depending on the gene) is compared with the decrease observed in tumor cell density (1.8-fold), it is clear that the loss of gene expression is not simply due to the reduction in cell number following treatment. In agreement with the real-time PCR data, wild-type *Ptc1* mRNA was present at relatively low levels in the tumor tissue, and its expression did not change after drug treatment (Figure 3). The control gene, *Reln*, was still expressed at high levels in tumor present in the drug-treated mice. Thus, HhAntag selectively suppressed Shh pathway target genes in vivo by blocking Smo signaling in medulloblastoma cells, with complete suppression at 100 mg/kg given twice a day.

HhAntag affects morphology and growth of *Ptc1*$^{+/-}$*p53*$^{-/-}$ medulloblastoma

Since HhAntag effectively blocked Smo activity in mice treated for 4 days, we analyzed the morphology of treated tumors. Neuropathological examination readily distinguished among tumors from untreated and 20 or 100 mg/kg of HhAntag-treated mice (Figure 4A). Although all tumors were composed of small round cells with oval to carrot-shaped hyperchromatic nuclei and minimal surrounding cytoplasm, those in the treated mice less often formed large, confluent tumor masses. The lesions in treated mice more often manifest as small collections of individual tumor cells in the superficial confines of the cerebellar molecular layer. The most striking difference observed among the three groups was a dramatic decrease in mitotic activity (Figure 4B). Immunohistochemical staining with the Ki67 marker for cell proliferation confirmed the observation that HhAntag decreased the proliferative index in tumor tissues ($p < 0.0001$, Exact Kruskall-Wallis) (Figure 4C). We also observed more cell death in tumors from treated mice, as indicated by increased numbers of pyknotic nuclei (Figure 4B) and by TUNEL assay ($p = 0.0402$, Exact Kruskall-Wallis) (Figure 4C). The influx of macrophages and microglia into the drug-treated tumors (as determined by Mac2 immunohistochemistry) increased from

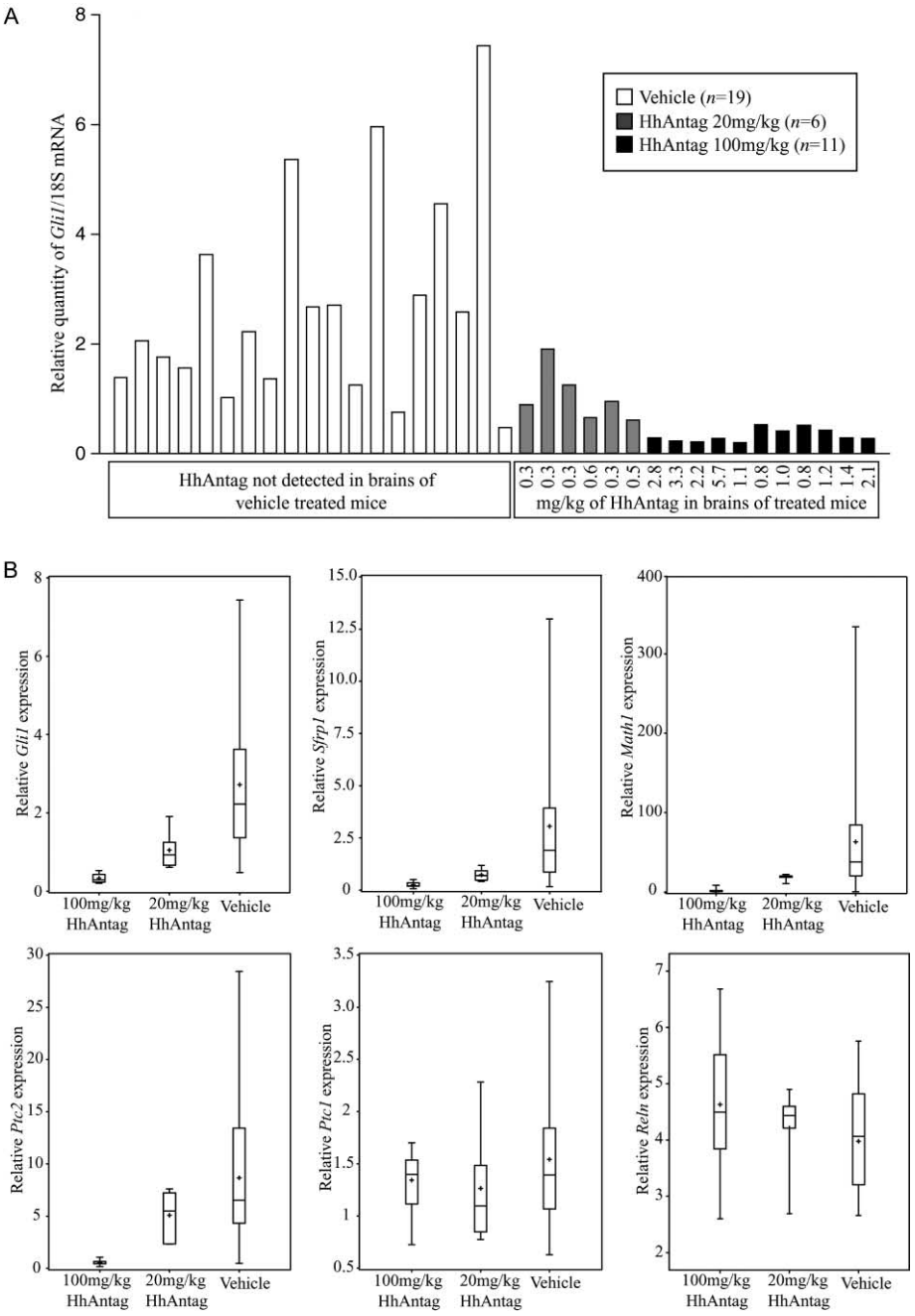

Figure 2. HhAntag suppresses the Shh pathway in mouse medulloblastoma in vivo

A: Real-time PCR analyses of total RNA isolated from tumor-bearing cerebella showing *Gli1* expression in mice treated twice daily for 4 days with HhAntag at 20 or 100 mg/kg or with vehicle alone. The amount of HhAntag present in each treated brain, 4 hr after the last dose, is indicated under each of the bars.

B: Box plots derived using Exact Kruskal-Wallis test to analyze gene expression in the treated brains showing that HhAntag suppressed *Gli1, Sfrp1, Math1*, and *Ptc2*, but not *Ptc1*. *Reln*, a gene expressed in medulloblastoma, but not under control of the Shh pathway, was analyzed as a control. Levels of mRNA for all assayed genes were within the linear range of a standard curve derived by amplifying each gene from serially diluted RNA, isolated from an independent source.

2.5% of Mac2-positive cells in vehicle-treated tumors to 5% and 7% in tumors treated with 20 and 100 mg/kg of HhAntag, respectively. Macrophage infiltration is associated with damage or loss of cells and it is not necessarily indicative of necrosis. In fact, necrosis was not observed in any of the tumors treated with HhAntag. HhAntag treatment also caused a dose-dependent increase in expression of the astrocyte marker, GFAP, which is characteristic of reactive gliosis often associated with CNS trauma. Taken together, the data presented above indicate that even a short-term treatment with HhAntag inhibited tumor growth.

After completion of treatment, we observed that, in the vehicle group, four out of five mice exhibited an overwhelming tumor burden and only one mouse had a small tumor. In contrast, in the cohort treated with 20 mg/kg of HhAntag, one mouse had a very large tumor, three had small tumors, and one had almost no tumor, whereas in the 100 mg/kg treatment group, one mouse had a large tumor, one had a medium-sized tumor, and three mice showed almost no tumor burden. Representative sagittal sections, taken through the largest tumor cross-section, are shown in Supplemental Figure S1. Although the short-term treatment with HhAntag appeared to inhibit tumor growth, the differences in tumor size between vehicle- and drug-treated mice were not dramatic. Therefore, we designed a study to

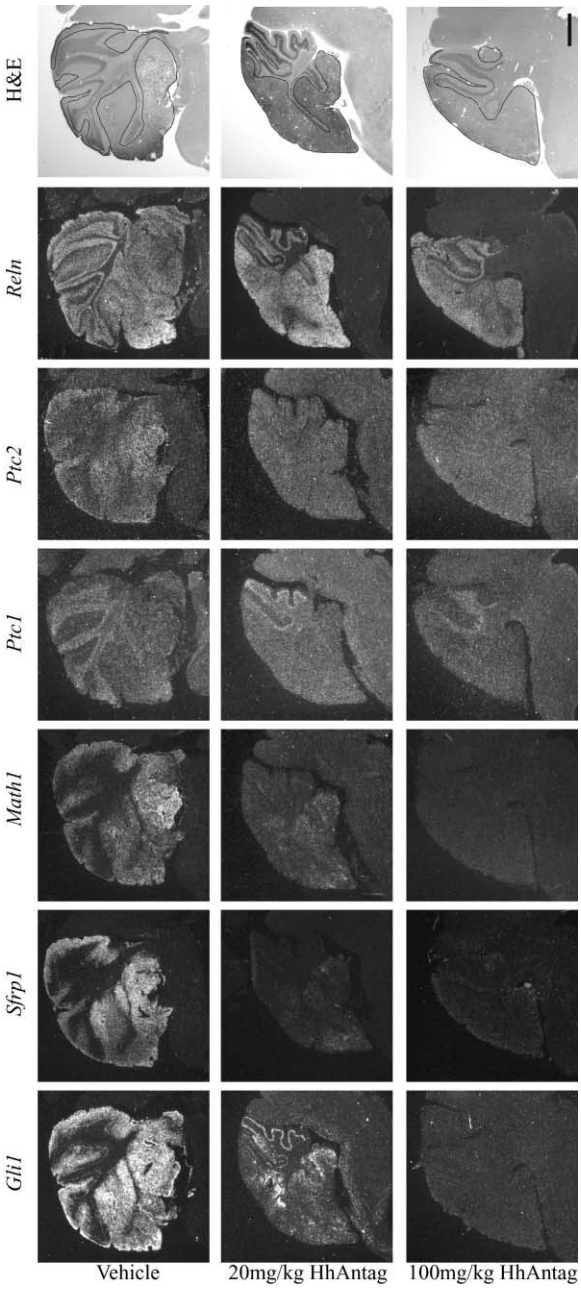

Figure 3. Treatment of *Ptc1*$^{+/-}$*p53*$^{-/-}$ mice with HhAntag suppresses *Gli1, Sfrp1, Math1,* and *Ptc2,* but not *Ptc1* in medulloblastoma

In situ hybridization analyses were performed using radiolabeled probes on brain tissue from *Ptc1*$^{+/-}$*p53*$^{-/-}$ mice. Expression of *Gli1, Sfrp1 Math1,* and *Ptc2* genes was downregulated after 4 days of treatment, twice daily with 20 mg/kg of HhAntag, and completely suppressed following treatment with 100 mg/kg HhAntag. *Ptc1* mRNA was present at low levels in the tumor and in the normal Purkinje cell and internal granule cell layers. Treatment with HhAntag did not alter the pattern or intensity of the *Ptc1* signal. *Reln* mRNA, highly expressed in medulloblastoma, did not change following treatment. The panels on the far right show adjacent paraffin sections of the tumor-bearing cerebella, stained with haematoxylin and eosin, tumor regions outlined. Scale bar equals 800 μm.

determine the effect of HhAntag on tumor volume in *Ptc1*$^{+/-}$ *p53*$^{-/-}$ mice treated for the extended period of 2 weeks.

HhAntag eliminates tumor mass in *Ptc1*$^{+/-}$*p53*$^{-/-}$ mice

To determine the effects of HhAntag on tumor growth, mice were treated for 14 days, twice daily, at either 20 or 100 mg/kg, or with vehicle alone. Treatment was initiated when mice were 3 weeks old, at which age all *Ptc1*$^{+/-}$*p53*$^{-/-}$ mice exhibit discernible tumor mass but not of a size that could adversely affect their health and short-term survival. At the end of the treatment period, brains were prepared for histological examination. We found that all the vehicle-treated mice had substantial tumor mass, whereas mice treated with 20 mg/kg of HhAntag had much smaller tumors and no tumor mass could be detected in the 100 mg/kg treatment group (Figure 5A). We used three-dimensional reconstruction analysis to measure tumor volumes by tracing sections at 150 μm intervals through the cerebellum (Figures 5B and 5C). Both the remaining normal IGL and the tumor areas were traced, and the tracings were aligned using the IGL as a guide to reconstruct tumor volume in 3D (Figures 5D and 5E). This is illustrated as a 3D computer-generated image with the IGL in blue (Figure 5D) and the tumor volume in several colors (Figures 5D and 5E). The IGL volume was subtracted in Figure 5E to clearly identify the total tumor volume in this example. Quantitative analysis revealed a marked decrease of tumor size in mice treated with 20 mg/kg HhAntag and a complete elimination of measurable tumor volume following treatment with 100 mg/kg HhAntag (Figure 5F). There was variation in the tumor mass present in the untreated cohort (5.6–34.8 mm^3) and in the 20 mg/kg treated mice (0.11–7.56 mm^3). The range of volumes was greater in untreated mice, as indicated by the standard deviation of 12.8 compared to 2.9 for the 20 mg/kg treated mice. The overall reduction in tumor volumes following treatment with HhAntag was examined using the Exact Kruskall-Wallis test; the Monte Carlo estimate of the p value (<0.0001) suggests a highly statistically significant differences in tumor volume distribution among the three treatment groups. We also found that there was a dose-dependent effect of HhAntag on tumor volume as indicated by the Exact Wilcoxon-Mann-Whitney test ($p = 0.0159$). There was an approximate 7-fold reduction in tumor volume between the untreated mice and mice treated with 20 mg/kg HhAntag (from an average of 19 mm^3 to 2.5 mm^3). Strikingly, complete tumor regression was observed following treatment of mice with 100 mg/kg HhAntag. In two of the four mice treated, no tumor remained at all. However, we did observe small lesions, indicating evidence of regression in the most lateral aspect of the cerebellum of the other two mice (Figure 5G). These areas showed no evidence of proliferation and they contained scattered apoptotic bodies and focal reactive changes, particularly lymphocyte infiltrate from leptomeningeal blood vessels. The lesions were confined to the molecular layer and the subpial zone. Thus, HhAntag, given twice daily at 100 mg/kg, effectively eliminated medulloblastoma in *Ptc1*$^{+/-}$*p53*$^{-/-}$ mice.

HhAntag prolongs brain tumor-free survival of *Ptc1*$^{+/-}$*p53*$^{-/-}$ mice

To determine if HhAntag could prolong survival of *Ptc1*$^{+/-}$*p53*$^{-/-}$ mice, we treated 20 5-week-old mice with either 100 mg/kg of the drug or vehicle, once daily for an extended period. The dose was lower than used in the previous studies because of limited

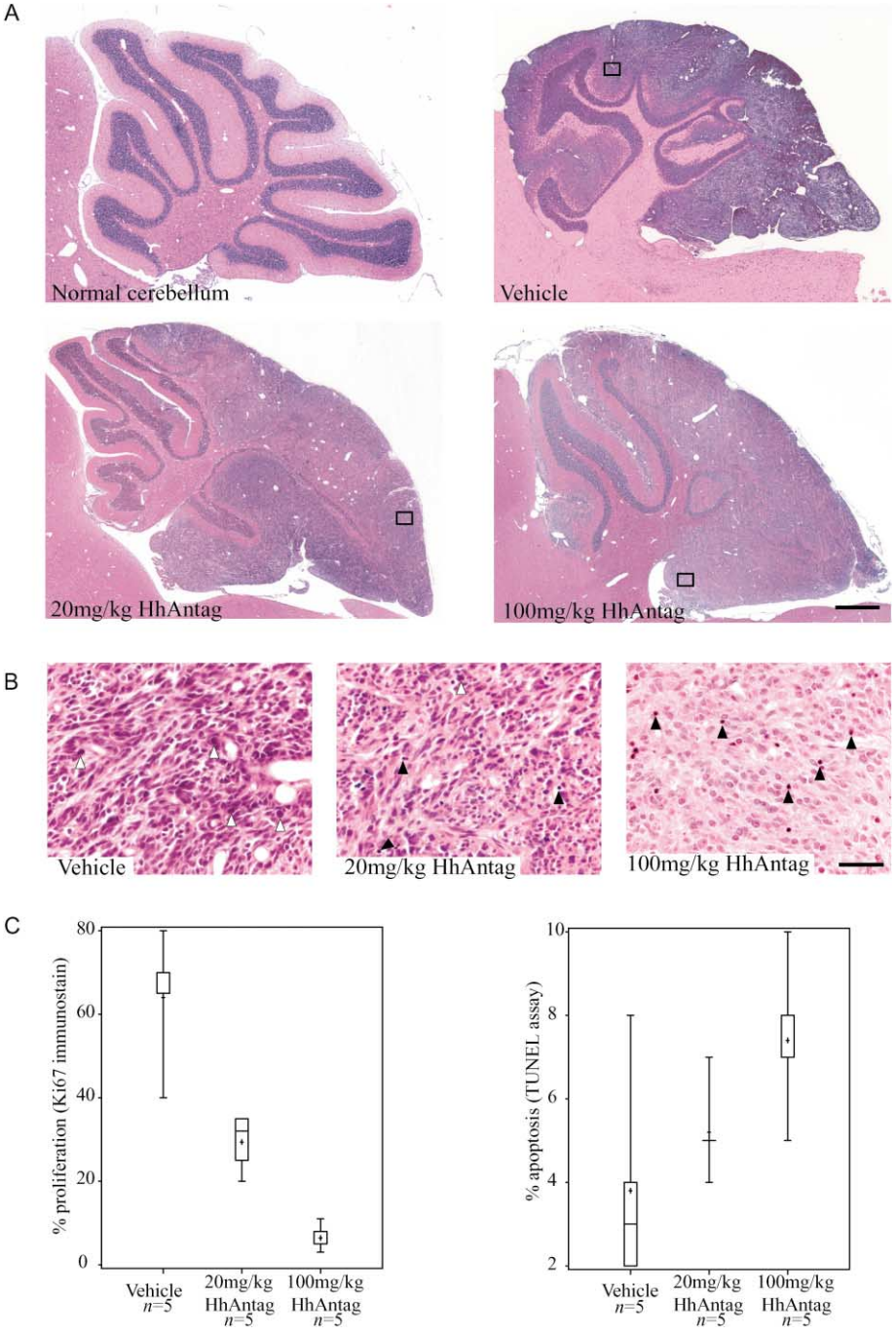

Figure 4. HhAntag inhibits proliferation, increases apoptosis, and alters morphology of medulloblastoma cells in vivo

A: Sections of brain tissue from mice treated twice daily with vehicle or HhAntag at 20 or 100 mg/kg, at low magnification. Scale bar equals 500 μm.

B: High magnification of **A**. Scale bar equals 50 μm. The locations of the regions examined at high magnification are indicated by black boxes. Note the increase in apoptotic bodies (black arrowheads) and the decrease in mitotic figures (white arrowheads) associated with HhAntag treatment. All sections were stained with haematoxylin and eosin.

C: Quantitative analyses of proliferation and apoptosis in tumors are presented as box plots. The data were obtained by counting Ki67- (proliferation) and TUNEL- (apoptosis) positive cells in the drug- and vehicle-treated mice. The data were analyzed using the Exact Kruskall-Wallis tests, with Monte Carlo estimates of p values of <0.0001 for proliferation and 0.0402 for apoptosis, suggesting statistically significant difference among the three treatment groups.

availability of the HhAntag compound and the concern that prolonged, twice daily delivery of the drug by oral gavage could result in injury. Also due to the limited availability of HhAntag, four of the ten mice receiving HhAntag were removed from drug after 50 days of treatment. All mice treated with vehicle alone developed clinical signs of brain tumors, such as domed head, ataxia, and tilting of the body, and were euthanized between 4 and 74 days after the start of treatment. In contrast, drug-treated mice survived significantly longer (39 to 147 days), and only five mice were euthanized due to brain tumors (Figure 6). Three of these had received HhAntag for only 50 days. The remaining five mice in the treated cohort were euthanized after exhibiting symptoms of other tumors typical of *p53* null mice, including thymic lymphomas, soft tissue sarcomas, and teratomas. However, each of these mice also showed evidence of small medulloblastomas when the brain was removed and examined. These results indicate that treatment of mice with 100 mg/kg of HhAntag once daily did not completely eliminate medulloblastoma. This is most probably because the dose of drug used, while sufficient to retard tumor growth, was not high enough to cause total regression. Nevertheless, analyses of the data revealed that HhAntag significantly extended the period of brain tumor-

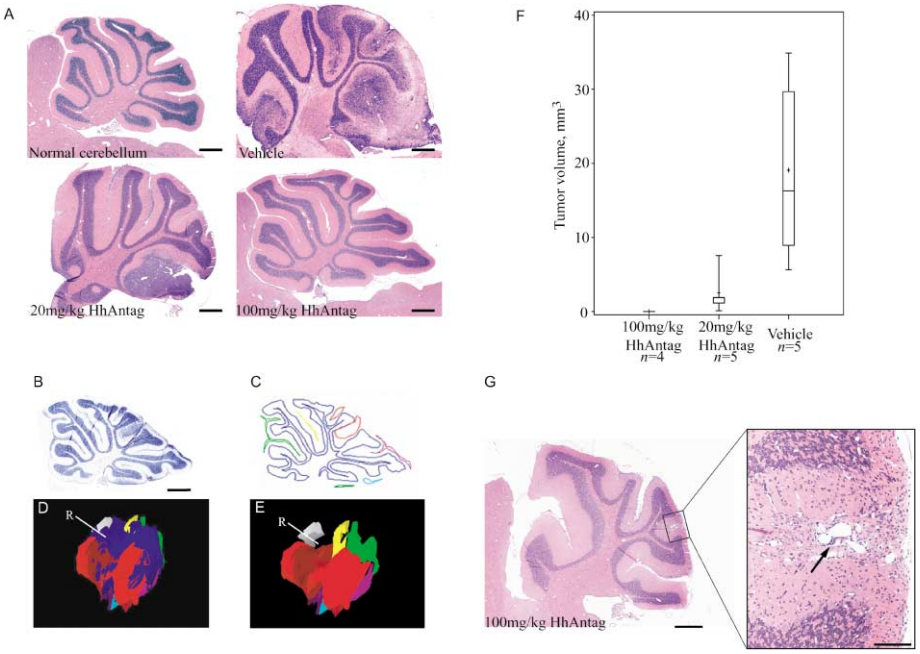

Figure 5. HhAntag given twice daily eliminates tumor mass in vivo

A: Sections of brain tissue from a wild-type mouse (normal cerebellum) and *Ptc1*$^{+/-}$*p53*$^{-/-}$ mice treated twice daily with vehicle or HhAntag at 20 or 100 mg/kg are shown. Treatment was initiated at three weeks of age. Scale bar equals 500 μm.

B–E: Determination of tumor volumes using the Bioquant Nova 3D reconstruction program.

B: An example of a 5 μm sagittal section from an untreated *Ptc1*$^{+/-}$*p53*$^{-/-}$ mouse, stained with cresyl violet. Scale bar equals 500 μm.

C: The outline of the IGL is indicated by the blue trace, and the regions of tumor are traced in the other colors. The different colors used for tracing the tumor area mark separate regions of tumor.

D and E: Sections were traced every 150 μm and assembled to create 3D images of the tumor (**D**) plus the IGL or the tumor alone (**E**). R, rostral direction.

F: Tumor volumes from vehicle-treated mice and from mice treated with HhAntag at 20 or 100 mg/kg are represented in a box plot. The Exact Kruskall-Wallis test suggests a clear statistical difference in the distribution of tumor volumes among the three groups ($p < 0.0001$), and the Exact Wilcoxon-Mann-Whitney test revealed statistically significant dose-dependent decrease in tumor volume associated with HhAntag treatment ($p = 0.0159$).

G: Signs of tumor regression are present in some mice treated with 100 mg/kg of HhAntag, twice daily for 14 days. The figure shows a low-power image in the left panel and a high-power view in the right panel of a lesion area (boxed in the low-power image). Infiltrating lymphocytes are indicated by a black arrow. Scale bar equals 500 μm for the low-power and 100 μm for the high-power image. All sections were stained with haematoxylin and eosin unless indicated otherwise.

free survival in *Ptc1*$^{+/-}$*p53*$^{-/-}$ mice (the Exact Two-Sided p value for Log-Rank Test was 0.0001).

Discussion

In this study, an inhibitor of the Shh pathway, HhAntag, eliminated tumor in a mouse model of spontaneous medulloblastoma. HhAntag blocked the ability of Smo to increase *Gli1* expression in tumor cells and reduced tumor cell proliferation in vivo. At the highest dose used, there was no measurable tumor volume after 2 weeks of treatment. Remarkably, although tumor growth disrupts the structure of the cerebellum, cerebellar morphology was relatively normal in the treated mice. These findings provide strong encouragement for the development of small molecules that block Smo function to treat tumors in which the Shh pathway is activated. Our findings extend previous studies using cultured tumor cells and transplantable tumors in which cyclopamine was shown to inhibit growth of mouse and human tumor cells (Berman et al., 2002, 2003; Taipale et al., 2000; Thayer et al., 2003). However, we also demonstrate that the Shh pathway is downregulated in cultured mouse medulloblastoma cells and that inhibition of cell proliferation in culture using cyclopamine and HhAntag is not mediated by inhibition of Smo. In contrast, treatment of mice with HhAntag blocked tumor growth at the same concentration that inhibited Smo activity, as determined by the level of *Gli1* expression. This finding suggests that additional factor(s), present in the intracranial environment but missing in cell culture, are required to maintain the ability of tumor cells to respond to Shh. These results underscore the utility of genetically programmed mouse tumor models in which effects of targeted therapies can be determined in an appropriate in vivo context.

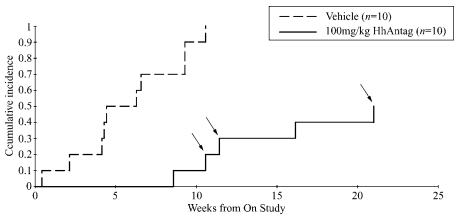

Figure 6. Treatment of *Ptc1*$^{+/-}$*p53*$^{-/-}$ mice with HhAntag increases life expectancy

At 5 weeks of age, mice were arbitrarily assigned into two groups of ten. One cohort was treated once daily with 100 mg/kg of HhAntag, and the other with vehicle alone. The graph shows the cumulative incidence of euthanasia due to brain tumors in the presence of competing event: euthanasia due to other tumors. The Exact two-sided p value for the log-rank test was 0.0001, indicating a highly significant difference in brain tumor-free survival between HhAntag- and vehicle-treated mice. Due to the limited amount of drug available, after 50 days of treatment, drug was withheld from four of the eight mice still alive in the treatment group. Three of these mice subsequently developed medulloblastoma (the times of euthanasia are indicated by arrows).

HhAntag penetrated the blood-brain barrier after oral delivery and efficiently suppressed tumor cell proliferation. Although apoptosis was increased in treated tumors, particularly at the highest dose used, this effect was modest. It is likely that the major mechanism of action of HhAntag is antiproliferative; how-

ever, we cannot rule out the possibility that a peak of cell death occurs at an earlier time point during the treatment regime. The basal apoptotic rate in tumors is quite high, so inhibition of proliferation would result in loss of tumor volume by attrition. The loss of tumor volume was associated with macrophage infiltration and reactive gliosis but not necrosis. Future studies will address the temporal mechanism of action of HhAntag. During the course of our experiments, we did not detect any toxic side effects of the therapy. Even in prolonged studies, in which mice received 100 mg/kg of HhAntag every day for more than 50 days, there were no signs of deleterious effects or weight loss in the treated group.

Treatment of mice with HhAntag for 2 weeks at 100 mg/kg twice daily resulted in an absence of measurable tumor volume, suggesting that at this dose, the tumor was eradicated before drug resistance could develop. The high dose was crucial for the tumor response, as there was only a partial regression in the cohort of mice receiving 20 mg/kg. Furthermore, in the survival study, in which HhAntag was given at 100 mg/kg once a day, mice still succumbed to medulloblastoma, albeit with a significant delay compared to vehicle-treated mice. Thus, in considering the use of HhAntag for treating human disease, it will be important to use the appropriate dose to ensure complete suppression of Smo in tumor cells. Alternatively, it may be possible to identify additional inhibitors that display more favorable pharmacokinetics.

Although Gli1 is a target of Smo signaling, it is not yet known if Gli1 mediates the oncogenic activity of the Shh pathway. Recently, it was reported that a virus expressing Shh is capable of inducing medulloblastoma in mice lacking *Gli1* (Weiner et al., 2002). Since *Gli2* is functionally similar to *Gli1*, there may be redundancy and/or compensation among family members (Bai et al., 2002; Park et al., 2000). However, in addition to suppression of *Gli1*, we found that HhAntag also inhibited expression of several other genes in tumor cells in vivo, including *Gli2* (data not shown). It is possible that some or all of these genes contribute directly to oncogenesis. At present, it is not possible to distinguish between cause and effect: the changes in gene expression could be responsible for the effect on tumor growth, or the inhibition of tumor growth might have resulted in the changes in gene expression. We are now pursuing time course experiments and gene expression microarray studies to examine the differences in gene expression between treated and untreated mice. These studies will help to decipher the mode of action of HhAntag.

We were surprised to discover that, in contrast to *Gli1*, *Math1*, *Ptc2*, and *Sfrp1*, the level of *Ptc1* was not reduced after treatment with HhAntag. This was not expected, as *Ptc1* is induced in cell culture, including medulloblastoma cell cultures, by overexpression of *Gli1*. Previously, we reported that the wild-type *Ptc1* allele is expressed in medulloblastoma at a similar level to that observed in normal P7 and adult cerebellum (Wetmore et al., 2000, 2001). These findings contrasted with a report using reverse-transcriptase PCR analysis to indicate that expression of *Ptc1* is lost in medulloblastoma (Berman et al., 2002). These authors concluded that complete loss of *Ptc1* expression was necessary for medulloblastoma formation. However, our observation was confirmed by an independent study (Zurawel et al., 2000), and we have now extended these analyses using quantitative real-time PCR, in situ hybridization, Northern blotting (data not shown), and microarray analysis (Lee et al., 2003). Additionally, complete sequencing of the normal *Ptc1* allele, using cDNA from tumors and tumor cell lines, demonstrated that the remaining *Ptc1* allele is not mutated. Therefore, haploinsufficiency of *Ptc1* promotes medulloblastoma formation in $Ptc1^{+/-}$ and $Ptc1^{+/-}p53^{-/-}$ mice. In tumor cells, *Ptc1* is not subject to the usual positive feedback regulation, as *Ptc1* levels, unlike those of *Gli1*, are not downregulated following suppression of the Shh pathway by the Smo inhibitor HhAntag in vivo. This implies that there may be a defect in the autoregulatory loop of the Shh pathway in tumor cells in vivo.

The three-stage preclinical approach we devised to explore the effect of a small molecule inhibitor in our mouse model may have general application. In the first stage, we carried out a short-term study demonstrating that HhAntag inhibited its target, Smo, in tumor cells in vivo in a dose-dependent manner. The second stage involved longer-term exposure of mice to the compound followed by quantitative evaluation of the dose-dependent effects of HhAntag on tumor growth. The final stage, similar to human clinical trials, demonstrated that prolonged exposure improved the survival of mice with tumors. At each stage, the drug was delivered by oral gavage to mimic the potential dosing route in patients. To apply this approach, it is critical to develop a high-incidence, early-onset mouse model, consistent with the genetics of human tumors. It is likely that such models represent only one particular molecular subtype of the tumor, rather than the entire spectrum of the corresponding human disease. In our case, the activated Shh pathway in tumor cells allowed testing of the proof of principle that inhibition of Smo by a targeted therapy would block tumor growth in vivo. For this strategy to be successful, it is important to identify a reliable marker of pathway activity (*Gli1* expression level in our case) and to use compounds with good bioavailability in the target tissue. If these conditions can be met, the three-stage approach described here can provide information on dose-dependent activity, tumor pathology, potential side effects, and long-term survival.

Since HhAntag works by suppressing Smo activity, it should be effective against medulloblastomas in which upstream components of the Shh pathway have been activated by mutation. However, HhAntag may also have a broader application. Several mouse medulloblastoma models have been described in which *p53*, together with *PARP-1*, *Lig4*, *Rb*, or different cell cycle regulators have been mutated (Hesselager and Holland, 2003; Lee et al., 2003). These tumors exhibit similar gene expression profiles to $Ptc1^{+/-}$ medulloblastoma, including elevated *Gli1* levels, indicating that they may also be inhibited by HhAntag (Lee et al., 2003). Approximately 25% of sporadic human medulloblastoma harbor mutations in different components of the Shh pathway (Ellison et al., 2003). These tumors are excellent candidates for potential treatment with Smo inhibitors, and it is also possible that some of the remaining 75% of human medulloblastoma would respond to HhAntag. Inhibitors of the Shh pathway may also be efficacious against other tumors with an activated Shh pathway, such as most basal cell carcinoma (Aszterbaum et al., 1998), a subset of meningioma, breast carcinoma, and colon cancer (Xie et al., 1997). Suppression of Shh signaling could also be beneficial in tumors that do not harbor mutations in the Shh pathway, but in which Shh signaling is important for continuous tumor cell growth (Berman et al., 2003; Thayer et al., 2003).

The data presented here provide strong support for initiating

human clinical trials with molecular inhibitors of the Shh pathway, such as the Smo suppressor HhAntag. The patient populations most likely to benefit from such intervention would include Gorlin syndrome patients and patients with sporadic medulloblastoma containing mutations in the Shh pathway. One important challenge in such trials would be to identify a marker that could serve as an indicator for dose-dependent suppression of Smo signaling. This could be achieved by monitoring changes in gene expression, for example, downregulation of *Gli1*. However, it may be necessary to utilize surrogate cells affected by the treatment, for example, epidermal cells in which the Shh pathway is active, or alternative tumor-specific markers such as secreted proteins that could be measured in blood or cerebral spinal fluid, to monitor the efficacy of pathway suppression.

Ultimately, it is likely that success in treating cancer will require the use of several compounds in concert that target distinct pathways important for tumor cell growth. Our mouse studies with HhAntag offer the hope that such precise, targeted molecular interventions could spare children from the devastating effects of surgery, toxic chemotherapy, and exposure to high doses of radiation.

Experimental procedures

Cell culture, luciferase, and cell growth assays

Mouse medulloblastoma cell cultures were established and characterized as previously described (Li et al., 2003). NIH3T3 and medulloblastoma cell cultures were maintained in DMEM (GIBCO-BRL/Invitrogen) under standard conditions. Cells were plated at 4×10^4 or 1×10^4 per well in a 24-well plate 24 hr before transfection. 0.25 μg of *Gli*-Firefly luciferase reporter plasmid (Sasaki et al., 1997) and 0.0125 μg of *Renilla* luciferase plasmid (pRL-SV40) mixed with Fugene 6 were applied to the cells (Roche Diagnostics). Cells were harvested 48 hr after transfection medium containing 0.5% FBS, ShhN, and HhAntag compound (Curis, Inc., Boston, MA) was applied to confluent cells. Luciferase assays were performed according to manufacturer's instructions (Dual Luciferase Assay Kit, Promega) and normalized for transfection efficiency using *Renilla* luciferase activity.

Cell proliferation was assayed in triplicates using Alamar blue reagent according to the manufacturer's directions. HhAntag was obtained from Curis. HhAntag is available from Genentech under a material transfer agreement, available at http://www.gene.com/gene/about/collaborations/contracts.jsp. HhAntag details are presented in the US patent WO 2003011219, available from the web site http://l2.espacenet.com/espacenet/viewer?PN=WO03011219.

Retroviral vectors and retroviral-mediated gene transfer

HA-tagged, full-length mouse *Gli1* cDNA was generated by PCR and subcloned into pCX4pur retroviral-mediated expression vector (GenBank accession #AB086386). Retroviral-mediated gene transfer was performed as described previously (Akagi et al., 2003). 72 hr after the infection, cells were harvested and used for the Northern blotting analyses.

Cerebellar granule neuron precursor culture and BrdU incorporation assay

Cerebellar granule neuron precursor cells were isolated from postnatal day 6 C57Bl/6 mice as previously described (Furuya et al., 1998) and plated at a density of 3×10^5 cells/cm^2 onto poly-D-lysine-coated plastic plates (BD Bioscience), with indicated amounts of ShhN and HhAntag. 10 μM BrdU was added 2 hr before cells were fixed with 0.5 M HCl, 70% EtOH. BrdU assays were performed using BrdU labeling and detection kit III (Roche Diagnositcs) according to manufacturer's instructions.

Northern blot analysis

Total RNA was isolated from snap frozen tissue or cultured cells using the TriPure reagent (Roche Diagnostics), according to the manufacturer's instructions. 10 μg was separated on 1% agarose gel under denaturing conditions and transferred onto nylon membrane (Hybond-N$^+$, Amersham Biosciences). After UV crosslinking, the membrane was hybridized using DNA probes for *Gli1* (NM_010296.1) nt966–2664, *Ptch1* (NM_008957.1) nt4191–4305 plus the 739 nucleotides of the 3′UTR, *Ptch2* (NM_008958.1) nt652–3549, and *Smo* (NM_176996.3) nt2824–3962.

Mice

The mice used in this study were generated and maintained on a mixed C57Bl/6;129Sv background, as described previously (Wetmore et al., 2001). Mice were observed daily and euthanized according to NIH-approved institutional guidelines when showing signs of increased intracranial pressure or extracranial tumors were evident. Animals were housed in an American Association of Laboratory Animal Care-accredited facility and maintained in accordance with the NIH Guidelines for the Care and Use of Laboratory Animals. The Institutional Animal Care and Use Committee at St. Jude Children's Research Hospital approved all procedures for animal use.

Real-time PCR analysis of gene expression

6-week-old *Ptc1*$^{+/-}$*p53*$^{-/-}$ mice treated by oral gavage twice daily for 4 days, with HhAntag at 20 or 100 mg/kg or vehicle. 4 hr following the last dose, mice were euthanized and their tumor-bearing cerebella were snap frozen in liquid nitrogen. Total RNA was extracted using the TriPure reagent (Roche Diagnostics). 5 ng was analyzed using the real-time RT-PCR ABI Prism 7900 sequence detection system (Applied Biosystems). Levels of assayed genes were normalized to 18S rRNA abundance. The sequences of the amplification primers and Taqman probes are: *Gli1* primers 5′-GCT TGGATGAAGGACCTTGTG, 5′-GCTGATCCAGCCTAAGGTTCTC, probe 5′-CCGGACTCTCCACGCTTCGCC; *Sfrp1* primers 5′-TCCTCCATGCGACA ACGA, 5′-TGATTTTCATCCTCAGTGCAAACT, probe 5′-TGAAGTCAGAGG CCATCATTGAACATCTCTG; *Math1* primers 5′-ATGCACGGGCTGAACCA, 5′-TCGTTGTTGAAGGACGGGATA, probe 5′-CCTTCGACCAGCTGCGCA ACG; *Ptc1* primers 5′-CAAGTGTCGTCCGGTTTGC, 5′-CTGTACTCCGAGT CGGAGGAA, (detecting the wt *Ptc1* allele), probe 5′-CCTCCTGGTCACACG AACAATGGGTC; *Ptc2* primers 5′-TGGAGCCACCTTGGTACAAGA, 5′-GGC GCTCAGGAAAGCATGT, probe 5′-CTGGCCCTGACAGATGTGGTCCCT; and *Reln* primers 5′-GGCGATGCCCTGGTCTTTAT, 5′-TCTGTGACTGAGCA GGAGGCA, probe 5′-AAAAGGCCAGCACCCGTTACGTGG.

Pharmacokinetics

Brains were snap frozen 4 hr after the last HhAntag dose, homogenized in PBS, and centrifuged. HhAntag was extracted from the supernatant using a Strata-X solid phase extraction column (Phenomenex 8B-S100-UBJ). The drug was eluted with methanol/acetonitrile/acetic acid (70/30/0.012), dried, reconstituted with 100 μl 20% acetonitrile water, and centrifuged, and supernatant was transferred into an autosampler vial for injection. Chromatographic separation was achieved on a Waters Xterra MSC_{18} 3.5 μm, 30 × 2.1 mm column with an isocratic mobile phase of acetonitrile and water (50:50). The analytes were detected with a triple quadrupole mass spectrometer, and the ions were monitored in the multiple reaction monitoring (MRM) mode including m/z 451 (precursor ion) to m/z 150.9 (product ion) for HhAntag and m/z 328 (precursor ion) to m/z 244 (product ion) for HhAntag-585 (internal standard). The lower limit of quantitation of HhAntag was 5 ng/ml (signal/noise ≥ 5), and results from a 5-day validation study demonstrated acceptable within-day and between-day precision (CV% values ≤4.4% and ≤5.5%, respectively) and accuracy (range 104.4% to 108.0%).

In situ hybridization

Gene expression was evaluated by in situ hybridization as described previously (Rice et al., 1998). Probes for *Gli1*, *Ptch1*, and *Ptch2* are described above; *Sfrp1* (NM_013834.1) nt239–1200, *Math1* (NM_007500.2) nt602–1128, *Reln* (NM_011261.1) nt5269–5975. Probes were [α-^{33}P]UTP radiolabeled. Autoradiography proceeded for 1–10 days. Reference sections were stained with hematoxylin and eosin. Slides were photographed with a Nikon Coolsnap ES camera mounted onto a Zeiss Stemi 11 Stereo microscope.

Histological analyses

Mice were perfused intracardially with 4% paraformaldehyde and brains were removed and postfixed overnight at 4°C. Brains were dehydrated through a series of ethanols, delipidated in mixed xylenes, and embedded in Paraplast X-TRA (Fisher Scientific). Brains were sectioned at 5 μm in the sagittal plane and mounted on Superfrost+ slides (Fisher Scientific). For

histological analyses, sections were stained with haematoxylin and eosin using standard histological protocols. Slides were photographed using Axioplan Zeiss microscope (Zeiss) and RT color SPOT camera (Diagnostic Instruments).

Volumetric measurement of tumors

Stained sections taken every 150 μm were analyzed using the Bioquant Nova Advanced Image Analysis software. An outline of the remaining normal IGL and the tumor region was prepared for every section. This analysis was inclusive in that any abnormal tissue area was assumed to be tumor. Traces were aligned using the IGL outline as a reference and reconstructed into a three-dimensional image, and the volume for every tumor was calculated.

Immunohistochemistry and detection of apoptosis

Paraffin sections were processed for immunohistochemistry with antibody against Ki67 (Novocastra Laboratories) by deparaffinization and rehydration followed by antigen retrieval in 10 mM sodium citrate at 80°C. Slides were treated with 1% H_2O_2, blocked in 10% normal goat serum, and incubated with primary antibody (1:2000 dilution) overnight at room temperature. Immunoreactivity was detected using the ABC Elite kit (Vector Laboratories) and diaminobenzidine reagent set (Kirkegaard and Perry Laboratories), according to manufacturers' recommendations. Slides were cover-slipped and analyzed using an Olympus BX60 microscope. Cells undergoing apoptosis were detected using the DeadEnd Colorimetric TUNEL system (Promega), according to manufacturer's instructions. Proliferative and apoptotic indexes were determined by counting 900–1300 cells for each tumor.

Survival studies

A cohort of 25-week-old *Ptc1*$^{+/-}$*p53*$^{-/-}$ mice was treated with HhAntag at 100 mg/kg of body weight, or vehicle alone, by oral gavage, once daily. The mice were observed daily and euthanized if any sign of illness could be discerned. The presence of brain tumors was confirmed by gross examination of dissected brain.

Statistical considerations for the manuscript

StatXact-5 for Windows was used for all exact statistical analyses (Statistical Software for Exact Nonparametric Inference, CYTEL Software Corporation). The assumption that gene expression intensities were from Gaussian distributions was rejected by the exact Shapiro-Wilk's test (all p values < 0.05); thus, the traditional t test is not valid for analyzing these data. Exact Kruskal-Wallis tests were used to compare gene expression intensities, levels of proliferation and apoptosis, as well as tumor volumes between vehicle and treated mice. Cumulative incidence functions of mice euthanized due to brain tumors in the presence of competing events of euthanasia due to other tumors were estimated as discussed by Kalbfleisch and Prentice and compared using exact log-rank tests. All p values are for two-sided tests and those less than 0.05 were considered statistically significant without adjustment for multiple testing (Kalbfleisch and Prentice, 1980; Kruskal and Wallis, 1952; Shapiro and Wilk, 1965).

Acknowledgments

We thank the members of the Curran Lab for discussions and comments on the manuscript. We thank Youngsoo Lee for help with the real-time PCR analyses. We thank James Boyett and Mehmet Kocak for statistical analysis of the data. We thank Peter Burger and Charles Eberhart (Johns Hopkins University) for advice on pathology. S.G. and L.L.R. are employees of Curis, Inc., a publicly traded biotechnology company. This work was supported by CA096832, NS036558, CA-021765, Cancer Center Support (CORE) grants from the National Institutes of Health and by the American Lebanese and Syrian Associated Charities (ALSAC).

Received: June 29, 2004
Revised: August 2, 2004
Accepted: August 19, 2004
Published: September 20, 2004

References

Akagi, T., Sasai, K., and Hanafusa, H. (2003). Refractory nature of normal human diploid fibroblasts with respect to oncogene-mediated transformation. Proc. Natl. Acad. Sci. USA *100*, 13567–13572.

Aszterbaum, M., Rothman, A., Johnson, R.L., Fisher, M., Xie, J., Bonifas, J.M., Zhang, X., Scott, M.P., and Epstein, E.H., Jr. (1998). Identification of mutations in the human PATCHED gene in sporadic basal cell carcinomas and in patients with the basal cell nevus syndrome. J. Invest. Dermatol. *110*, 885–888.

Bai, C.B., Auerbach, W., Lee, J.S., Stephen, D., and Joyner, A.L. (2002). Gli2, but not Gli1, is required for initial Shh signaling and ectopic activation of the Shh pathway. Development *129*, 4753–4761.

Berman, D.M., Karhadkar, S.S., Hallahan, A.R., Pritchard, J.I., Eberhart, C.G., Watkins, D.N., Chen, J.K., Cooper, M.K., Taipale, J., Olson, J.M., and Beachy, P.A. (2002). Medulloblastoma growth inhibition by hedgehog pathway blockade. Science *297*, 1559–1561.

Berman, D.M., Karhadkar, S.S., Maitra, A., Montes De Oca, R., Gerstenblith, M.R., Briggs, K., Parker, A.R., Shimada, Y., Eshleman, J.R., Watkins, D.N., and Beachy, P.A. (2003). Widespread requirement for Hedgehog ligand stimulation in growth of digestive tract tumours. Nature *425*, 846–851.

Binns, W., James, L.F., Shupe, J.L., and Everett, G. (1963). A congenital cyclopian-type malformation in lambs induced by maternal ingestion of a range plant, *Veratrum californicum*. Am. J. Vet. Res. *24*, 1164–1175.

Chen, J.K., Taipale, J., Cooper, M.K., and Beachy, P.A. (2002). Inhibition of Hedgehog signaling by direct binding of cyclopamine to Smoothened. Genes Dev. *16*, 2743–2748.

Chintagumpala, M., Berg, S., and Blaney, S.M. (2001). Treatment controversies in medulloblastoma. Curr. Opin. Oncol. *13*, 154–159.

Cooper, M.K., Porter, J.A., Young, K.E., and Beachy, P.A. (1998). Teratogen-mediated inhibition of target tissue response to Shh signaling. Science *280*, 1603–1607.

Corcoran, R.B., and Scott, M.P. (2001). A mouse model for medulloblastoma and basal cell nevus syndrome. J. Neurooncol. *53*, 307–318.

Ellison, D. (2002). Classifying the medulloblastoma: insights from morphology and molecular genetics. Neuropathol. Appl. Neurobiol. *28*, 257–282.

Ellison, D.W., Clifford, S.C., Gajjar, A., and Gilbertson, R.J. (2003). What's new in neuro-oncology? Recent advances in medulloblastoma. Eur. J. Paediatr. Neurol. *7*, 53–66.

Frank, A.J., Hernan, R., Hollander, A., Lindsey, J.C., Lusher, M.E., Fuller, C.E., Clifford, S.C., and Gilbertson, R.J. (2004). The TP53-ARF tumor suppressor pathway is frequently disrupted in large/cell anaplastic medulloblastoma. Brain Res. Mol. Brain Res. *121*, 137–140.

Furuya, S., Makino, A., and Hirabayashi, Y. (1998). An improved method for culturing cerebellar Purkinje cells with differentiated dendrites under a mixed monolayer setting. Brain Res. Brain Res. Protoc. *3*, 192–198.

Gabay, L., Lowell, S., Rubin, L.L., and Anderson, D.J. (2003). Deregulation of dorsoventral patterning by FGF confers trilineage differentiation capacity on CNS stem cells in vitro. Neuron *40*, 485–499.

Goodrich, L.V., and Scott, M.P. (1998). Hedgehog and patched in neural development and disease. Neuron *21*, 1243–1257.

Goodrich, L.V., Milenkovic, L., Higgins, K.M., and Scott, M.P. (1997). Altered neural cell fates and medulloblastoma in mouse patched mutants. Science *277*, 1109–1113.

Gorlin, R.J. (1995). Nevoid basal cell carcinoma syndrome. Dermatol. Clin. *13*, 113–125.

Hahn, H., Wicking, C., Zaphiropoulous, P.G., Gailani, M.R., Shanley, S., Chidambaram, A., Vorechovsky, I., Holmberg, E., Unden, A.B., Gillies, S., et al. (1996). Mutations of the human homolog of *Drosophila* patched in the nevoid basal cell carcinoma syndrome. Cell *85*, 841–851.

Hesselager, G., and Holland, E.C. (2003). Using mice to decipher the molecular genetics of brain tumors. Neurosurgery *53*, 685–695.

Johnson, R.L., Rothman, A.L., Xie, J., Goodrich, L.V., Bare, J.W., Bonifas, J.M., Quinn, A.G., Myers, R.M., Cox, D.R., Epstein, E.H., Jr., and Scott, M.P. (1996). Human homolog of patched, a candidate gene for the basal cell nevus syndrome. Science *272*, 1668–1671.

Kalbfleisch, J.D., and Prentice, R.L. (1980). Statistical Analysis of Failure Time Data (New York: Wiley).

Keeler, R.F., and Binns, W. (1968). Teratogenic compounds of *Veratrum californicum* (Durand). V. Comparison of cyclopian effects of steroidal alkaloids from the plant and structurally related compounds from other sources. Teratology *1*, 5–10.

Kimonis, V.E., Goldstein, A.M., Pastakia, B., Yang, M.L., Kase, R., DiGiovanna, J.J., Bale, A.E., and Bale, S.J. (1997). Clinical manifestations in 105 persons with nevoid basal cell carcinoma syndrome. Am. J. Med. Genet. *69*, 299–308.

Kleihues, P., Schauble, B., zur Hausen, A., Esteve, J., and Ohgaki, H. (1997). Tumors associated with p53 germline mutations: a synopsis of 91 families. Am. J. Pathol. *150*, 1–13.

Kruskal, W.H., and Wallis, W.A. (1952). Use of ranks in one-criterion variance analysis. J. Am. Stat. Assoc. *47*, 583–621.

Lee, Y., Miller, H.L., Jensen, P., Hernan, R., Connelly, M., Wetmore, C., Zindy, F., Roussel, M.F., Curran, T., Gilbertson, R.J., and McKinnon, P.J. (2003). A molecular fingerprint for medulloblastoma. Cancer Res. *63*, 5428–5437.

Li, L., Connelly, M.C., Wetmore, C., Curran, T., and Morgan, J.I. (2003). Mouse embryos cloned from brain tumors. Cancer Res. *63*, 2733–2736.

Malkin, D., Li, F.P., Strong, L.C., Fraumeni, J.F., Jr., Nelson, C.E., Kim, D.H., Kassel, J., Gryka, M.A., Bischoff, F.Z., Tainsky, M.A., et al. (1990). Germ line p53 mutations in a familial syndrome of breast cancer, sarcomas, and other neoplasms. Science *250*, 1233–1238.

Park, H.L., Bai, C., Platt, K.A., Matise, M.P., Beeghly, A., Hui, C.C., Nakashima, M., and Joyner, A.L. (2000). Mouse Gli1 mutants are viable but have defects in SHH signaling in combination with a Gli2 mutation. Development *127*, 1593–1605.

Reifenberger, J., Wolter, M., Weber, R.G., Megahed, M., Ruzicka, T., Lichter, P., and Reifenberger, G. (1998). Missense mutations in SMOH in sporadic basal cell carcinomas of the skin and primitive neuroectodermal tumors of the central nervous system. Cancer Res. *58*, 1798–1803.

Rice, D.S., Sheldon, M., D'Arcangelo, G., Nakajima, K., Goldowitz, D., and Curran, T. (1998). Disabled-1 acts downstream of Reelin in a signaling pathway that controls laminar organization in the mammalian brain. Development *125*, 3719–3729.

Sasaki, H., Hui, C., Nakafuku, M., and Kondoh, H. (1997). A binding site for Gli proteins is essential for HNF-3beta floor plate enhancer activity in transgenics and can respond to Shh in vitro. Development *124*, 1313–1322.

Shapiro, S.S., and Wilk, M.B. (1965). An analysis of variance test for normality (complete samples). Biometrika *52*, 591–611.

Taipale, J., Chen, J.K., Cooper, M.K., Wang, B., Mann, R.K., Milenkovic, L., Scott, M.P., and Beachy, P.A. (2000). Effects of oncogenic mutations in Smoothened and Patched can be reversed by cyclopamine. Nature *406*, 1005–1009.

Taipale, J., Cooper, M.K., Maiti, T., and Beachy, P.A. (2002). Patched acts catalytically to suppress the activity of Smoothened. Nature *418*, 892–897.

Taylor, M.D., Liu, L., Raffel, C., Hui, C.C., Mainprize, T.G., Zhang, X., Agatep, R., Chiappa, S., Gao, L., Lowrance, A., et al. (2002). Mutations in SUFU predispose to medulloblastoma. Nat. Genet. *31*, 306–310.

Thayer, S.P., di Magliano, M.P., Heiser, P.W., Nielsen, C.M., Roberts, D.J., Lauwers, G.Y., Qi, Y.P., Gysin, S., Fernandez-del Castillo, C., Yajnik, V., et al. (2003). Hedgehog is an early and late mediator of pancreatic cancer tumorigenesis. Nature *425*, 851–856.

Van Dyke, T., and Jacks, T. (2002). Cancer modeling in the modern era: progress and challenges. Cell *108*, 135–144.

Wechsler-Reya, R., and Scott, M.P. (2001). The developmental biology of brain tumors. Annu. Rev. Neurosci. *24*, 385–428.

Weiner, H.L., Bakst, R., Hurlbert, M.S., Ruggiero, J., Ahn, E., Lee, W.S., Stephen, D., Zagzag, D., Joyner, A.L., and Turnbull, D.H. (2002). Induction of medulloblastomas in mice by sonic hedgehog, independent of Gli1. Cancer Res. *62*, 6385–6389.

Wetmore, C., Eberhart, D.E., and Curran, T. (2000). The normal patched allele is expressed in medulloblastomas from mice with heterozygous germline mutation of patched. Cancer Res. *60*, 2239–2246.

Wetmore, C., Eberhart, D.E., and Curran, T. (2001). Loss of p53 but not ARF accelerates medulloblastoma in mice heterozygous for patched. Cancer Res. *61*, 513–516.

Williams, J.A., Guicherit, O.M., Zaharian, B.I., Xu, Y., Chai, L., Wichterle, H., Kon, C., Gatchalian, C., Porter, J.A., Rubin, L.L., and Wang, F.Y. (2003). Identification of a small molecule inhibitor of the hedgehog signaling pathway: effects on basal cell carcinoma-like lesions. Proc. Natl. Acad. Sci. USA *100*, 4616–4621.

Xie, J., Johnson, R.L., Zhang, X., Bare, J.W., Waldman, F.M., Cogen, P.H., Menon, A.G., Warren, R.S., Chen, L.C., Scott, M.P., and Epstein, E.H., Jr. (1997). Mutations of the PATCHED gene in several types of sporadic extracutaneous tumors. Cancer Res. *57*, 2369–2372.

Zurawel, R.H., Allen, C., Wechsler-Reya, R., Scott, M.P., and Raffel, C. (2000). Evidence that haploinsufficiency of Ptch leads to medulloblastoma in mice. Genes Chromosomes Cancer *28*, 77–81.